Available online at www.sciencedirect.com
SCIENCE DIRECT
Polymer 47 (2006) 1678–1688
polymer
www.elsevier.com/locate/polymer

On the structure and morphology of polyvinylidene fluoride–nanoclay nanocomposites

Douglas R. Dillon [a], Kishore K. Tenneti [a], Christopher Y. Li [a,*], Frank K. Ko [a], Igors Sics [b], Benjamin S. Hsiao [b]

[a] A.J. Drexel Nanotechnology Institute and Department of Materials Science and Engineering, Drexel University, Philadelphia, PA 19104, USA
[b] Department of Chemistry, State University of New York at Stony Brook, Stony Brook, NY, USA

Received 15 November 2005; received in revised form 27 December 2005; accepted 4 January 2006

Abstract

Polyvinylidene fluoride (PVDF)–nanoclay nanocomposites were prepared by both solution casting and co-precipitation methods with the nanoclay loading of 1–6 wt%. The structure and morphology of the nanocomposite were investigated by wide angle X-ray diffraction (WAXD), polarized light microscopy and transmission electron microscopy (TEM) techniques. PVDF phase transformation behavior was investigated using differential scanning calorimetry and in situ thermal WAXD. All the three typical nanoclay morphologies, namely, exfoliated, partially intercalated and phase separated morphologies, were observed in the PVDF–nanoclay nanocomposites prepared by different methods. In solution-cast samples, phase separation and intercalation occurred depending upon the organic modifiers while complete exfoliation of the nanoclays was observed in the co-precipitated nanocomposites. Furthermore, unique parallel orientation of the nanoclay layers and polymer film surface was achieved in solution-cast samples. β-form PVDF was observed in all the nanocomposites regardless of the nanoclay morphology and contents. Both crystallization and melting temperatures of PVDF were increased with the addition of nanoclay, possibly due to the formation of the β-form PVDF.

Keywords: Polymer nanoclay nanocomposite; PVDF; Polymer crystallization and morphology

1. Introduction

In the past decade, polymer-layered silicate (often referred as nanoclays) nanocomposites have proven to be an effective method of improving the physical properties of many different polymers [1–5]. Even at very low nanoclay loadings, these nanocomposites have achieved higher moduli, improved thermal properties, and better barrier properties for both thermoplastic and thermoset polymers [3,4]. They have also found commercial uses in such diverse applications as automobile engine components and plastic beverage containers [3,4]. While many polymer–nanoclay systems have been studied extensively, polyvinylidene fluoride (PVDF) composites have received relatively little attention. PVDF is a semicrystalline thermoplastic with applications in such diverse fields as paint for skyscrapers, transducers for sensitive scientific instruments, and pipes for caustic chemical byproducts [6,7]. Its CH_2–CF_2 repeat unit occupies a fascinating half-way point in the homologous series of fluorinated vinyl monomers stretching from polyethylene (PE) to the perfluorinated poly(tetrafluoroethylene) (PTFE). PVDF is typically 50–70% crystalline with five distinct crystal polymorphs named α, β, γ, δ, and ε [6–9]. This polymorph is directly related to the slightly larger van der Waals radius of fluorine (1.35 Å) versus hydrogen (1.2 Å). These different forms are fundamental to the unique properties and rich microstructure of PVDF and among the five polymorphs, the β-phase is most intriguing due to its piezo-, pyro- and ferroelectric properties, which can be attributed to the all trans conformation of the polymer chains [6–8]. A variety of experimental techniques have been developed to induce β-phase formation. Miller and Raisoni reported that solution crystallization of PVDF using cyclohexanone (~0.02%) over a narrow range of crystallization temperatures (T_c) produced β-form single crystals [10], while the results were questioned by Grubb and Choi [11]. Okuda et al. [12] and Toida and Chujo [13] reported that crystallization in dimethylsulfoxide also produced β-form single crystal while Cortili and Zerbi showed that the crystals belong

* Corresponding author. Tel.: +1 215 895 2083; fax: +1 215 895 6760.
E-mail address: chrisli@drexel.edu (C.Y. Li).

0032-3861/$ - see front matter © 2006 Elsevier Ltd. All rights reserved.
doi:10.1016/j.polymer.2006.01.015

to γ-form [14]. Lovinger obtained the β-form using melting crystallization on the (001) surface of freshly cleaved KBr [15]. Doll and Lando repoted that crystallization at 280 °C and higher than 5 kbar yielded β-form [16,17]. Matsushige and Takemura showed that crystallization from the melt above 3.5 kbar led to the formation of β-form PVDF (through solid state α–β transition or melting of α at 286 °C and recrytsallization of β at 274 °C, ~4 kbar) [18,19]. Uniaxial or biaxial drawing at ~50–100 °C induces α–β transition [20,21]. Strong electric field also induces α–β transition as first reported by Luongo [22], and later confirmed by Southgate [23], and Das-Gupta and Doughty [24,25]. Gal'perin and Kosmynin demonstrated the α–β transition was also achievable by using γ irradiation at 500 Mrad or more [26,27]. Carbon confined thin film crystallization has also been shown to be able to induce α–β transition [28]. Most recently, it was shown that nanoclay also induces PVDF β-form formation [29–36].

The first published data on PVDF–nanoclay nanocomposites was reported by Priya and Jog [29–31]. Solef 1008 resin from Solvay and two slightly different nanoclays [Cloisite® 6A (6A) and Cloisite® 20A (20A)] were used with the nanoclay contents of 1.5, 3, 5, and 7%. Melt intercalated polymer–nanoclay composites were prepared by blending nanoclay with PVDF in a Brabender plasticorder batch mixer. The 1.5 and 3% 6A samples are intercalated while the 5 and 7% samples are partially exfoliated. Despite the similarities of 6A and 20A, the wide angle X-ray diffraction (WAXD) results suggested the intercalation yield of PVDF/6A nanocompoiste is much lower than that of PVDF/20A nanocomposite. The crystallization rate of the composites was reported to be much higher than that of pristine PVDF. Liu et al. explored the use of montmorillonite (MMT)-based organically modified MMT nanoclays in conjunction with higher molecular weight (M_w = 530,000 g/mol) PVDF [32]. Both solid nanocomposites and gel PVDF–nanoclay nanocomposites containing lithium perchlorate ($LiClO_4^-$) salt were prepared by solution casting onto glass plates from DMF solutions. Nanocomposites containing 3 wt% or less were exfoliated while those containing 5 wt% or greater were intercalated. Gel polymer electrolytes were able to maintain their solvent longer under vacuum and they showed higher ionic conductivity. Liu argued that the higher conductivity was likely the result of increased cation (Li^+) mobility resulting from higher amorphous content and increased disassociation of the lithium perchlorate salt due to the organophilic modifier attracting the perchlorate (ClO_4^-) ion. Despite this argument, no evidence of decreased crystallinity was presented. Kim and White investigated PVDF–nanoclay nanocomposites as part of a study on a series of nanocomposites using nanoclay with various fluorinated polymers [33,34]. Using unmodified nanoclay (Cloisite® Na^+) as well as the same PVDF (Solvay's Solef 1008) and organically modified montmorillonite (Southern Nanoclay Products' 20A) as Priya and Jog, they also created nanocomposites by melt intercalation in a Brabender batch mixer. The WAXD data showed that there was no intercalation of PVDF when the unmodified nanoclay was used. The organically modified nanoclay was shown to be exfoliated at 3 wt% nanoclay, and intercalated at higher nanoclay loadings. This is in agreement with Priya and Jog's work.

Giannelis et al. have recently reported on the outstanding physical properties of Cloisite® 30B (30B) nanoclay and Kynar 721 (Arkema Inc.) PVDF nanocomposite [35]. These nanocomposite samples were prepared by melt-intercalation via twin screw extrusion. WAXD and TEM data demonstrated that the nanocomposites exhibited an intercalated morphology where the basal plane diffraction from the nanoclay increased from 1.8 to 2.9 nm. Using unmodified sodium montmorillonite showed no evidence of intercalation or exfoliation. It was noted that PVDF preferentially crystallizes in the β polymorph in the presence of the silicates. They also reported that the tendency of PVDF to crystallize in the β-phase increased as the nanoclay changed from unmodified to increasingly organically modified. Giannelis et al. suggested that the tendency of organically modified nanoclay to stabilize the β polymorph could be the result of similar crystal lattices between the nanoclay and the β polymorph, and the large flat surface of the nanoclay permitting intimate interaction between the polymer and inorganic components. Of interest is that neither neat nor organically modified silicate nanospheres promote the crystallization of the β polymorph. Unlike Priya and Jog, Giannelis and coworkers reported that there is no increase in either the crystal melting temperature (T_m) or a decrease in crystallinity with the addition of nanoclay and the change in the predominant crystal phase.

Using a twin-screw extruder, Pramoda et al. melt-compounded Nanocor Inc. I.34TCN nanoclay into Solvay's Solef® PVDF at 0, 1, 2 and 5 wt% [36]. Film samples for testing were compression molded at 190 °C and 1700 psi, then quenched to room temperature. WAXD and transmission electron microscopy (TEM) experiments showed that the nanoclay was exfoliated for the 2% sample, but contains at least some intercalation at 5% nanoclay. The PVDF–nanoclay composites showed an increasing fraction of β-phase as the nanoclay loading increased, but there always remains a significant amount of α-phase in the composites. This is in contrast to Priya and Jog and Giannelis et al. who showed nearly complete conversion to the β-phase upon addition of the nanoclay.

The aforementioned reports suggest the complicated phase behavior of PVDF–nanoclay nanocomposite system. Most of the reported PVDF–nanoclay nanocomposites were synthesized using melt compounding technique and intercalation occurs most frequently in these systems. In this paper, we report the structural and morphological behavior of PVDF–nanoclay nanocomposite prepared by both solution casting and co-precipitation methods. Two different nanoclay samples were employed and differential scanning calorimetry (DSC), polarized light microscopy (PLM), TEM and WAXD were employed to systematically investigate the structure and morphology of the nanocomposites. In situ thermal WAXD and DSC were also used to monitor the phase transformation of the nanocomposites. It was observed that the morphological behavior of the nanocomposite critically depends upon the sample preparation methods. Both well orientated nanoclay

sheets and completely exfoliated morphologies were successfully achieved and the detailed structure analyses were conducted.

2. Experimental

2.1. Materials

The powdered PVDF, obtained from Scientific Polymer Products, Inc., has a reported approximate weight-averaged molecular weight (M_w) of 530,000 g/mol. The organically modified MMT nanoclays were from Southern Clay Products, Inc. Cloisite® 15A (15A) contains 43 wt% dimethyl, dihydrogenated tallow and has a d_{001} spacing of 3.15 nm while Cloisite® 25A (25A) contains 34 wt% of organic modifier leading to a d_{001} spacing of 1.86 nm. These were confirmed experimentally through thermogravimetric analysis (TGA) and WAXD in our lab. The *N*,*N*-dimethylformamide (DMF) was A.C.S grade (99.8%) from Aldrich. All the materials described above were used directly without any further modification or treatment.

2.2. Sample preparation

Two different techniques were used to prepare the PVDF–nanoclay nanocomposites (1–6 wt%): (1) solution casting, and (2) co-precipitation. For PVDF samples with a given loading of a particular nanoclay, samples of both synthetic techniques were obtained from the same initial mixture as follows.

For each different percentage of nanoclay in PVDF, two premixes were made. One was for the nanoclay and the other was for the PVDF. The nanoclay/DMF premix was sonicated using a Branson 8510 ultrasonication bath at 30–40 °C for approximately 80 min. The PVDF premix was made using DMF as the solvent. The final solution was created by adding the contents of the nanoclay premix to the PVDF premix. The result was a mixture that is nominally 10 wt% PVDF/DMF with the desired percentage of nanoclay to PVDF.

After allowing it to cool to approximately 30–40 °C, this nominal 10% PVDF solution was used to create the solution cast samples as described below. The precipitated samples required a less viscous solution, so a volume of DMF approximately equivalent to the volume of the PVDF/nanoclay/DMF mixture remaining was added to the vial to create a nominal 5% solution suitable for precipitation. This procedure of using the same mixture for the two different synthetic techniques ensured a uniform nanoclay loading in the final composite, no matter which synthetic technique was used.

The solution cast samples were prepared by pouring a small amount of the warm (30–40 °C) nominal 10% PVDF solution from the vial onto a 2-in. diameter silicon wafer. The disc with solution was immediately placed into a glass dish, covered, and placed in an unheated vacuum oven at ambient pressure. Using the same solution, spin coating technique was also used with the spinning rate of 1000–1500 rpm. The precipitated samples were made using the more dilute nominal 5% solutions of PVDF/DMF. The mixture was poured into a cleaned, dried 250 mL beaker and swirled while 150 mL of deionized water was poured from a 125 mL Erlenmyer flask into the beaker. A stringy, white, translucent precipitate formed immediately. Then the precipitate and liquid was vacuum filtered in a Buchner funnel lined with filter paper. The precipitate was removed and placed on an aluminum foil weighing pan in the vacuum oven. Samples made by both techniques were dried in a vacuum oven for 48–72 h at approximately 80 °C. They were confirmed to be solvent-free by TGA.

For most physical testing, the precipitated samples needed to be pressed into films. Approximately, 0.1 g of precipitated sample was placed between mirror polished metal plates and pressed at 20 kpsi at 200 °C for 5 min, then the pressure was released while the sample remained between the heated plates (at 0 psi) for another 5 min. The sample and the polished plates were then placed in another press maintained at 10 °C and clamped lightly at less than 10 psi until cooled. The resultant samples were approximately 280 μm thick.

2.3. Instrumentation

TGA was performed using a Perkin–Elmer TGA-7. As noted in Section 3, either nitrogen or dry air at 30 mL/min was used to purge the approximately 3 mg sample while the temperature was ramped at 20 °C/min from 30 to 700 or 900 °C.

A Perkin–Elmer DSC-7 purged with nitrogen was used for DSC experiments. Each sample weighed approximately 4 mg. Typically, three 10 °C/min temperature scans were completed for each sample run, but only the last two are presented in the results. The first scan from 20 to 200 °C melted the sample. After holding at 200 °C for 1 min to remove any traces of crystalline structure, the sample was cooled back down to 20 °C to observe the crystallization exotherm upon cooling from the melt. Finally, the temperature was scanned to 200 °C to observe the melting endotherm.

PLM was performed on an Olympus BX51. The temperature of the sample was controlled to the nearest 0.1° with a Mettler Toledo FP82 HT hot stage controlled via the FP90 Central Processor. To view the morphology of the PVDF at a given crystallization temperature, the sample would first be melted at 200 °C for 3–5 min, then quenched to the crystallization temperature (T_c) and held for up to 12 h. PLM images could be taken at any crystallization time.

Two-dimensional (2D) WAXD analysis were performed using an imaging plate equipped with an 18 kW X-ray rotating anode generator (Cu Kα radiation, 1.54 Å, Rigaku automated X-ray imaging system with 1500×1500 pixel resolution). The air scattering was subtracted from the WAXD patterns. These tests were all performed at ambient conditions. In order to view the diffraction pattern more easily, integrations from the center out along the equator could be performed and plotted as a graph. The second type of WAXD analysis were in situ thermal experiments performed at Brookhaven National Laboratory's national synchrotron light source on beamline X27C. Generally, the sample was melted at 180 °C then cooled to 100 °C at 10 °C/min. During the cooling, XRD data was collected

between 10 and 40°. Each WAXD scan takes 30 s so that the sample temperature actually changed by 5 °C during the scan. However, to avoid confusion in the presentation of the data, each scan is defined by the temperature of the sample when the WAXD scan began. Upon reaching 100 °C, the sample was heated back up to 180 °C at 10 °C/min while continuing to collect data the same way that it was collected while cooling.

A JEOL 2000FX TEM with an accelerating voltage of 120 kV was used for the TEM experiments. A Reichert Ultracut cryo-ultramicrotome was used to prepare approximately 50 nm thick samples at room temperature, which were collected on Ni grids for TEM experiments.

3. Results and discussion

3.1. Phase morphology of PVDF–nanoclay nanocomposite

2D WAXD experiments were conducted on a solution-cast nanocomposite film and the film normal was defined as z, as shown in Scheme 1. X-ray was directed to the film either perpendicular (edgewise) or parallel (flat) to the z direction. The WAXD results in Fig. 1(a)–(c), were taken with the film samples aligned edgewise to the incident X-ray beam, as shown schematically in Fig. 1(e). Fig. 1(d) shows the WAXD pattern from the same sample as Fig. 1(c), but the sample was aligned flat to the incident X-ray beam (Fig. 1(e)). Using the same sample and exposing it to the incident X-ray radiation from these two perpendicular angles allowed us to determine the orientation of nanoclay layers in the nanocomposite film. In all the edgewise WAXD patterns, diffraction arcs can be observed on the equator in the low-angle regions while in the flat WAXD pattern (Fig. 1(d)), no diffraction was observed in the same region. Observing different WAXD patterns for the edgewise and flat sample set-up suggests that (1) both 15A and 25A were not exfoliated in these solution cast films, and (2) the nanoclay orientation in the composite film was not isotropic. Since, strong diffraction arcs were observed for the edgewise sample, this indicates that nanoclay layers are parallel to the film surface (Fig. 1(e)). When the X-ray was applied along the edgewise direction of the film, it was parallel to the nanoclay layers, leading to the strong diffraction arcs observed on the equator. In contrast, when X-ray was applied along the film normal, it was perpendicular to the nanoclay layers (Fig. 1(e)), whose diffractions were, therefore, out of the registration plane, leading to the absence of the low-angle diffraction in Fig. 1(d). Therefore, we conclude that in the solution-cast films, the nanoclay was not exfoliated and they were explicitly aligned

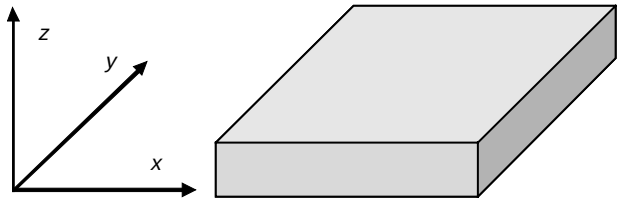

Scheme 1. Schematic representation of the coordinate geometry of a polymer nanocomposite film.

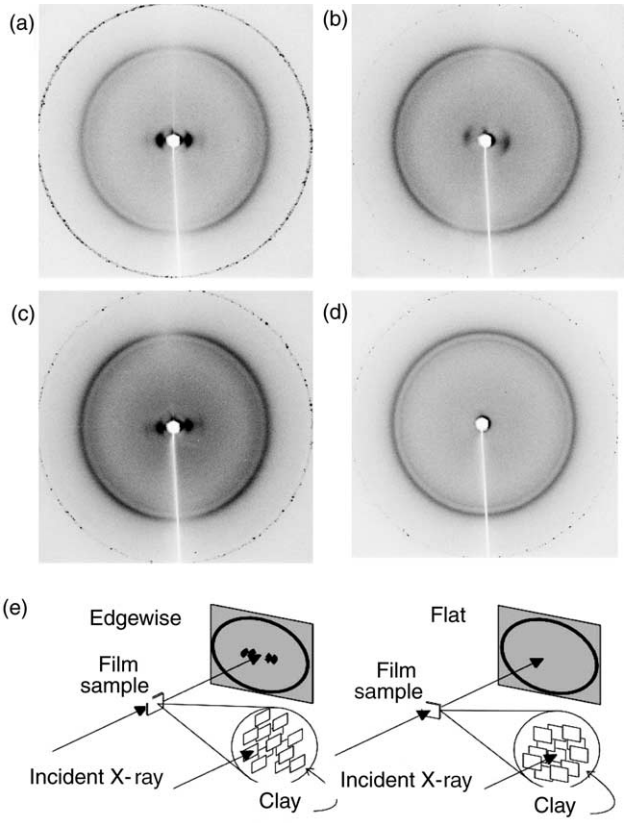

Fig. 1. Typical 2D WAXD images for solution-cast films of: (a) 4% 15A in PVDF aligned edgewise to X-ray beam, (b) 4% 25A in PVDF aligned edgewise to X-ray beam, (c) 2% 15A in PVDF aligned edgewise to X-ray beam, (d) 2% 15A in PVDF aligned flat to X-ray beam, and (e) schematics of edgewise and flat alignment of solution-cast film samples.

parallel to the film surface. This orientation is important because it leads to anisotropy in the physical properties of the composites. Most interestingly, this anisotropy places the plate-like silicate layers perpendicular to the direction of small molecule diffusion through the film thickness, perhaps providing the most effective gas diffusion barrier possible for this non-exfoliated morphology due to a much more tortuous path.

2θ integration along the equator from the center out to 10° for the images in Fig. 1(a) and (b) are shown in Fig. 2. The integrations demonstrate slightly different behavior for the nanoclays. The solution cast film containing 15A shows an average basal spacing (d_{001}) of 3.0 nm. Since, the basal spacing for neat 15A is 3.2 nm, it is thus evident that no PVDF polymer chains have intercalated between the silicate layers of the nanoclay. The fact that the nanoclay gallery spacing has actually decreased from that of the neat nanoclay suggests that the solution treatment used in making the composites likely altered the conformation of the organic modifier, which resulted in a slightly smaller gallery spacing. A solution-cast film made with a loading of 1–6 wt% 15A showed the same basal spacing as the 4% sample, indicating that, for solution-cast samples in the nanoclay concentration range explored, the loading of the 15A nanoclay does not affect the morphology or basal spacing and the nanocomposites are phase separated.

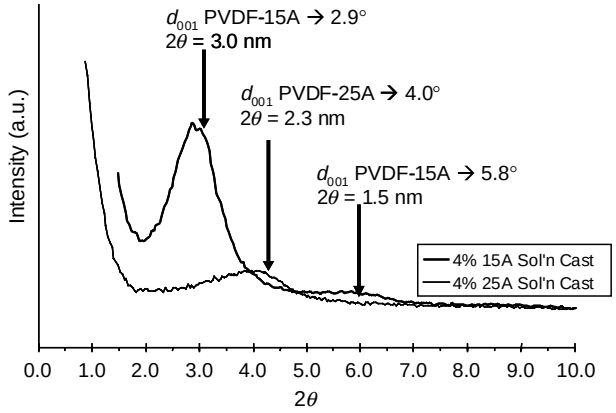

Fig. 2. 2θ integrations along the equator to 10° for solution cast films of 4% 15A in PVDF (Fig. 1(a)) and 4% 25A in PVDF (Fig. 1(b)).

There is also a second order peak at 5.8° (1.5 nm) in the WAXD pattern for the 15A sample. It should also be noted that spin-casting a 2% 15A sample at 1500 rpm showed the same morphology as the solution-cast sample.

25A is known to contain a lower loading (34 versus 43%) of a different, more hydrophobic modifier (dimethyl, hydrogenated tallow, 2-ethylhexyl quaternary ammonium chloride). The data for the composites made with this nanoclay shows some indication of partial exfoliation and partial intercalation. The intensity of the basal spacing peak of the 25A is much lower than the 4% 15A sample indicating that most of the silicate layers are exfoliated. The basal spacing of the remainder of the silicate layers is centered at 2.2 nm (4.0°) and ranges from approximately 1.8 to 3.0 nm. This range indicates that a slightly larger basal spacing than the 1.86 nm (4.75°) reported for the neat 25A, and no higher order peaks present. Partial intecalation morphology was thus achieved in solution-cast PVDF–25A nanocompoistes.

Since, nanoclay additives most effectively improve the physical properties of polymers when they are exfoliated, the solution cast samples, which were phase separated/partially intercalated for 15A and 25A, respectively, would likely show improved properties if the PVDF–nanoclay nanocomposite could be prepared with an exfoliated morphology. This was achieved by co-precipitation for both 15A and 25A nanocomposites as discussed in Section 2 and the results for 25A are shown in Fig. 3. The lack of a low angle peak from any ordered structure of the layered silicate in the 2D WAXD image of the precipitated 2% 25A sample shown in Fig. 3(a) clearly demonstrates that the precipitated sample is completely exfoliated. This is in contrast to the solution cast data shown in Fig. 3(b) which clearly has a partially intercalated structure with the nanophase platelets aligned parallel to the film surface (see previous discussion). The integrations along the right horizontal axis for these two samples are shown in Fig. 4. Inspecting only the low-angle region below 10°, it is immediately apparent that the solution cast sample is intercalated as evidenced by the broad peak that is centered near 5.9° (1.5 nm) and extends from the incident radiation halo below 3.5° (above 2.5 nm) to nearly 7° (1.2 nm). However, despite similar processing, this peak is much broader, less clearly defined, and shifted to a lower d-spacing (higher degrees) than the 4% 25A sample shown in Fig. 2, indicating partial intercalation of polymer into the nanoclay galleries. The precipitated sample containing 2% 25A shows no peaks arising from the layered silicates, indicating a completely exfoliated morphology with no preferred orientation of the silicate layers. A sample containing a higher loading of 4% 25A also demonstrated a completely exfoliated morphology, proving that co-precipitation is a viable method of creating an exfoliated PVDF–nanoclay nanocomposite.

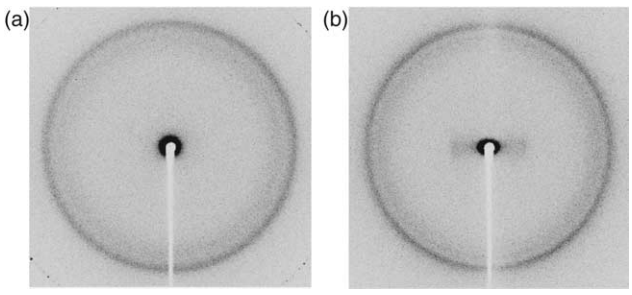

Fig. 3. 2D WAXD images of PVDF and PVDF–nanoclay nanocomposites: (a) precipitated 2% 25A sample, (b) solution cast 2% 25A sample.

We can thus conclude that there is a critical difference between the two different methods of nanocomposite preparation. Solution-cast samples showed a phase separated (for 15A)/partially intercalated (for 25A) morphology where the nanoclay maintained some level of long-range order in silicate layer tactoids, while the precipitated samples showed a completely exfoliated structure. Since, both the solution cast samples and the precipitated samples were created from the same initial solutions, discovering that the precipitated sample is exfoliated suggests that the DMF dissolution is adequate to completely exfoliate the nanoclays while in solution. The fact that a solution-cast film from the same solution dried over several hours or longer allows the exfoliated silicate layers sufficient time to self-assemble into partially intercalated tactoids suggests that the exfoliated structure resulting from precipitation is only a metastable structure. Thus, the kinetics of solidification plays an important role in determining the final composite morphology. The fast kinetics during precipitation freezes a metastable exfoliated morphology, while the slower

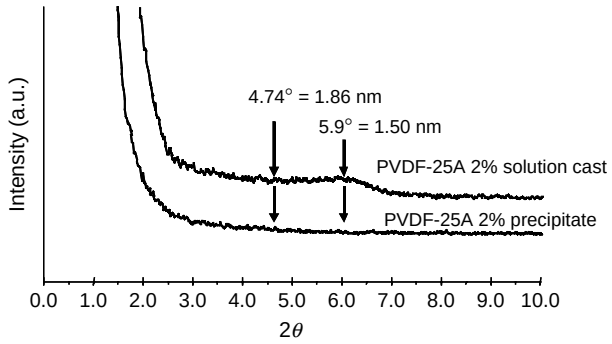

Fig. 4. The integrations along the equator of the 2D WAXD data shown in Fig. 3 clearly shows the different nanoclay morphology in a solution cast 2% 25A sample, and precipitated 2% 25A sample.

Fig. 5. TEM images of precipitated PVDF–nanoclay composite containing 2% 15A after hot-pressing into a film.

kinetics of evaporating solvent from solution cast films permits a more equilibrium intercalated or phase separated structure. The ability to control the morphology with kinetics permits the relatively easy fine-tuning of composite structure by changing processing conditions, rather than the more complex manipulation of polymer–nanoclay compatibility by changing the organic modifier, its loading, etc.

The physical form of the precipitate is a loose, white mat of fibers. Films of approximately 250 μm thick were prepared by hot-pressing the precipitate. WAXD experiments confirmed that mechanically pressing the precipitate into a film does not change the exfoliated morphology of the precipitated samples, which was also confirmed by the TEM experiment as shown in Fig. 5. The exfoliated silicate layers appear as sharp lines on a grey background from the PVDF matrix. The length of the silicate layers range from approximately 60 to 190 nm. Most of the nanoclays are fairly flat in the figure. It can also be seen that there are a few disorganized agglomerates of three to five silicate layers, but these lack a sufficient long-range order to give rise to low-angle WAXD peaks indicative of the intercalated/phase separated morphology.

3.2. PVDF crystal structure and morphology

Fig. 6 shows the 2θ integrations along wide angle regions of the equator for the solution-cast and precipitated samples presented in Figs. 1 and 3. As seen in the figure, in the 0% nanoclay precipitate sample, there are five peaks that clearly identify this sample as predominantly α-phase PVDF. The (020), (110) and (120)/(021) crystal planes for the α-phase at 18.6° (0.48 nm) and 20.3° (0.44 nm) and 27.6 (0.32 nm), respectively, are the most prominent and distinctive peaks. The

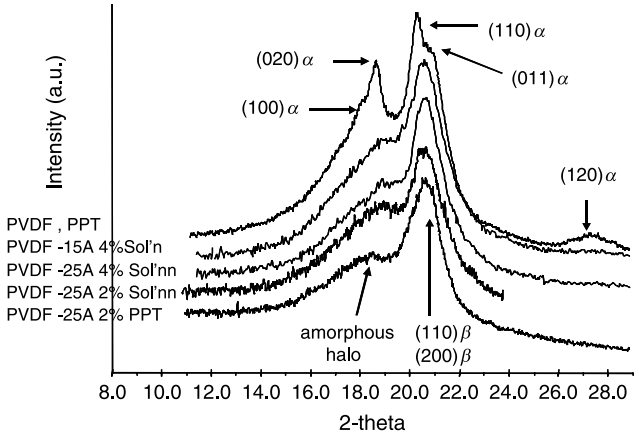

Fig. 6. The integrations along the equator from 11 to 25° of the 2D WAXD images shown in Fig. 1 clearly demonstrate that the presence of nanoclays in a nanocomposite leads to predominantly β-form PVDF.

α-phase (100) and (011) peaks appear as shoulders at approximately 17.7° (0.50 nm) and 20.8° (0.43 nm), respectively, on the two primary peaks. It is most interesting that the addition of either nanoclay, in any concentration, and with any resultant morphology from either of the two preparation methods, always promotes the crystallization of PVDF in the β polymorph. The WAXD patterns of all of the PVDF-layered silicate composites have a distinctly different feature than the pure PVDF sample; showing a single sharp peak at 20.7° (0.43 nm) from both the (110) and (200) crystal planes of the

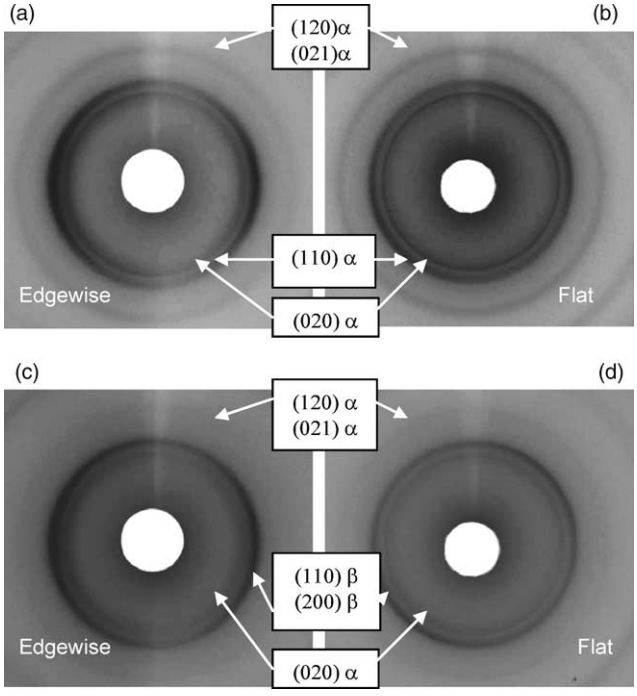

Fig. 7. 2D WAXD images of hot-pressed precipitate film samples: (a) pristine PVDF sample edgewise to X-ray beam, (b) pristine PVDF sample flat to X-ray beam, (c) PVDF–nanoclay nanocomposite with 2% 15A edgewise to X-ray beam, (d) PVDF–nanoclay nanocomposite with 2% 15A flat to X-ray beam.

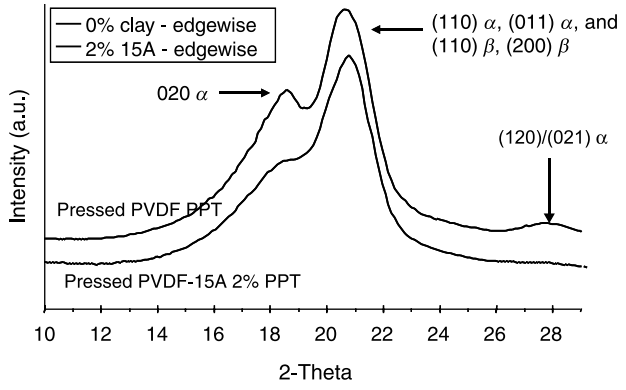

Fig. 8. 2θ integrations from approximately 10 to 30° 2θ of the images shown in Fig. 7 indicate that after hot-pressing the precipitates into films, the pristine PVDF samples predominantly retain α-phase and the PVDF–nanoclay nanocomposites predominantly retain β-phase.

β-phase overlapping the broad, amorphous halo centered near 18.6° (0.48 nm).

Fig. 7 shows the 2D WAXD patterns for hot-pressed pure PVDF and a PVDF–nanoclay nanocomposite with 2% 15A. The results of a 2θ integration that was performed on Fig. 7(a) and (c) between 10 and 32° are shown in Fig. 8 to facilitate the discussion of the PVDF crystal structure of precipitated samples after hot-pressing into films. Comparing Figs. 6 and 8 shows that hot-pressing the precipitated samples into films has only a very small effect on the overall crystalline structure of the PVDF. Pure PVDF samples predominantly retain α-phase as evidenced by the three distinctive peaks from the (020), (110) and (120)/(021) crystal planes at 18.6° (0.48 nm) and 20.3° (0.44 nm) and 27.6° (0.32 nm), respectively. Likewise, PVDF–nanoclay nanocomposites predominantly retain β-phase, as evidenced by the single peak at 20.7° (0.43 nm) from the (110) and (200) crystal planes of the β-phase overlapping the very broad, low, amorphous halo centered near 18.6° (0.48 nm).

3.3. Structure and morphological transformation of PVDF–nanoclay nanocomposites

The 2D WAXD data provides an excellent initial characterization of the structure and morphology of the PVDF–nanoclay nanocomposite. DSC, in situ thermal WAXD, and PLM were used to investigate the phase transformation of the nanocomposites.

3.3.1. Differential scanning calorimetry

Fig. 9 shows DSC thermograms for solution-cast and precipitated samples, which indicates that the addition of either

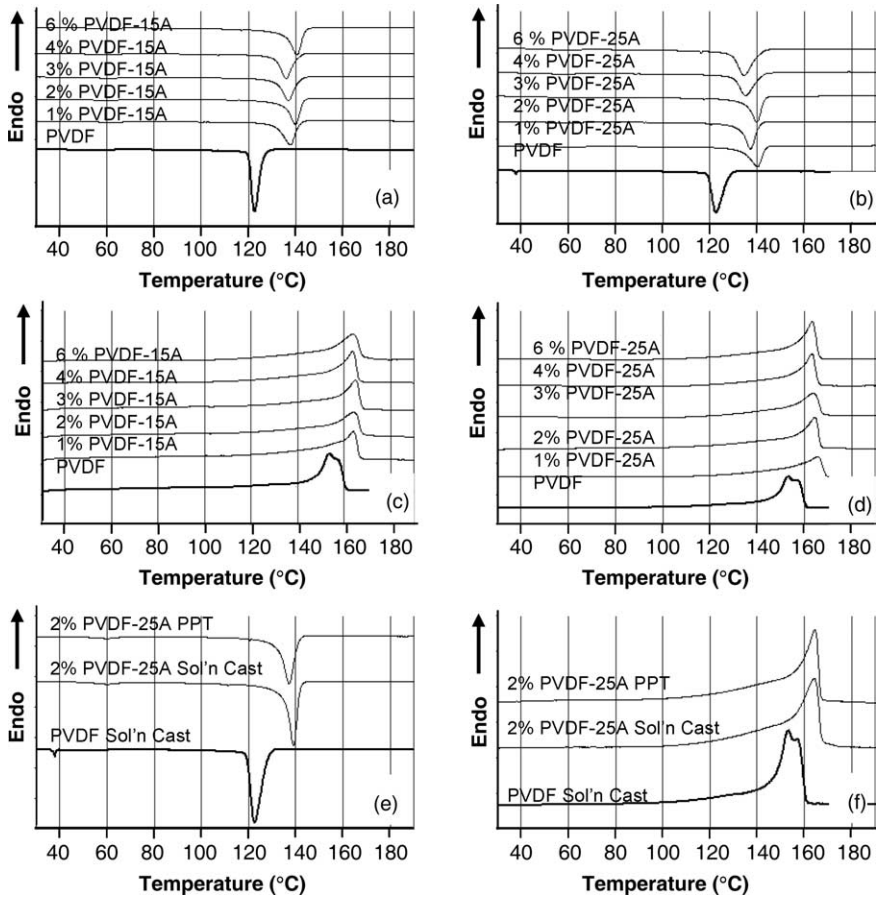

Fig. 9. Crystallization and melting DSC curves for: (a) cooling of PVDF and PVDF–15A precipitates, (b) cooling of PVDF and PVDF–25A precipitates, (c) heating of PVDF and PVDF–15A precipitates, (d) heating of PVDF and PVDF–25A precipitates, (e) cooling of PVDF, as well as 2% 25A precipitate and solution-cast samples, and (f) heating of PVDF, as well as 2% 25A precipitate and solution-cast samples.

Table 1
Tabulated DSC data for the crystallization and melting theromograms of solution cast films, precipitates, and hot-pressed precipitate films

	Crystallization exotherm data					Melting endotherm data		
	% Nanoclay	Peak (°C)	Onset (°C)	ΔH_{fus} (J/g)	% Crystallinity	Onset (°C)	Peak (°C)	ΔH_{fus} (J/g)
Sol'n cast film	0% Nanoclay	123	128	39.1	38	147	153	42.1
	2% 25A	139	142	35.6	35	153	164	39.6
Precipitate	0% Nanoclay	123	126	38.1	37	148	154	41.3
	1% 15A	138	142	32.3	31	156	164	42.8
	2% 15A	140	143	35.0	34	151	164	40.2
	3% 15A	137	141	32.6	32	156	165	41.7
	4% 15A	136	141	34.2	33	155	164	42.6
	6% 15A	140	144	37.5	36	151	164	40.1
	1% 25A	140	144	32.3	31	152	166	41.1
	2% 25A	137	141	34.0	33	155	164	45.3
	3% 25A	140	143	36.2	35	151	164	52.5
	4% 25A	135	142	34.8	34	156	163	46.3
	6% 25A	134	141	35.1	34	156	163	47.9
Hot-pressed	0% Nanoclay	122	125	39.5	38	147	153	48.4
PPT film	4% 15A	137	142	33.3	32	155	164	42.1

15A or 25A nanoclay dramatically increases T_c and T_m for both solution-cast and co-precipitated samples. This is detailed for a series of samples shown in Table 1 and Fig. 9 where T_c and T_m of pure PVDF are about 125–128 and 147–148 °C, respectively. The nanocomposites show more variability, but are consistently higher than the pure PVDF samples with T_c about 141–144 °C and T_m at about 151–156 °C. Fig. 10 shows the nanoclay content dependence of T_c and T_m. Given that the solution-cast samples are phase separated/intercalated, while the co-precipitated samples are exfoliated, it is of interest to note that there is no significant difference in their T_c or T_m. Further, T_c and T_m remain constant with increasing nanoclay content in the range explored (1–6 w/w%). All of this is consistent with the 2D WAXD data in the previous session, which shows that the addition of nanoclay promoted the crystallization of the β polymorph, which has higher T_c and T_m.

Table 1 also shows the calculated crystallinity (w_c) of PVDF and PVDF–nanoclay nanocomposites. For samples obtained from 10 °C/min cooling, the w_c of PVDF was ~38% while w_c of PVDF–nanoclay nanocomposites was ~31–36%. This crystallinity data is lower than that typically reported for commercial resins produced by Arkema and Solvay, and most likely is indicative of a higher head–head and tail–tail ratio in the PVDF used in this study versus commercially produced resins. The crystallinity remains relatively constant with nanoclay loading, regardless of the type of organic modifiers. There is also no difference whether the nanoclay is phase separated/intercalated as with the solution-cast samples or exfoliated as with the precipitated samples. Rather, the addition of any type, loading, or morphology of nanoclay within the range studied appears to uniformly promote β-phase crystallization while the presence of the silicate tactoids or exfoliated layers lowers total crystallinity. This could be the result of nanoconfinement provided by the nanoclay sheets. Table 1 also contains data from precipitated samples that were subsequently hot-pressed into films. T_c or T_m, and w_c for these samples are similar to the other PVDF and as-prepared PVDF–nanoclay nanocomposites [8]. The DSC curves are comparable to those prior to pressing and are shown in Fig. 11.

All DSC traces of melt crystallized pure PVDF—whether they are solution cast, precipitated, or a hot-pressed film—show two crystalline melting peaks as shown for the 0% nanoclay solution cast samples in Fig. 11. This is not the result of two distinct phases melting as evidenced by in situ WAXD

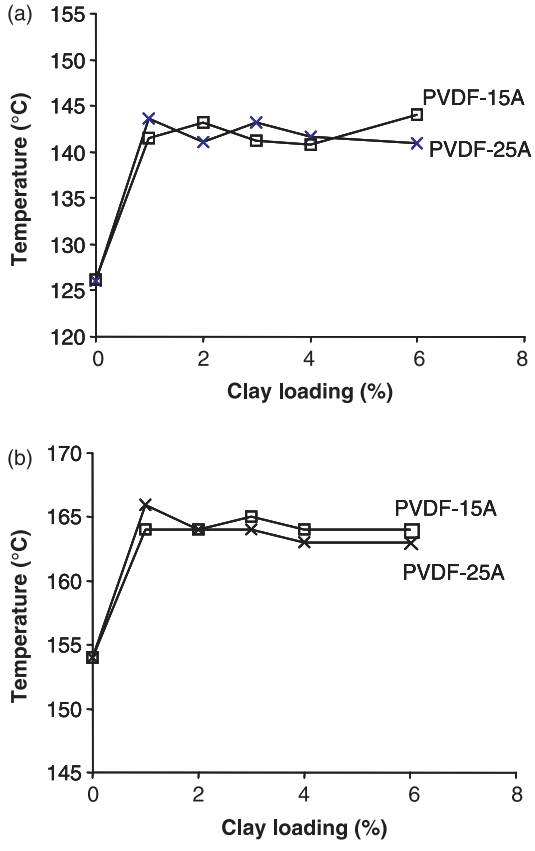

Fig. 10. Temperatures for: (a) crystallization, and (b) melting of PVDF and PVDF–15A and PVDF–25A nanocomposites.

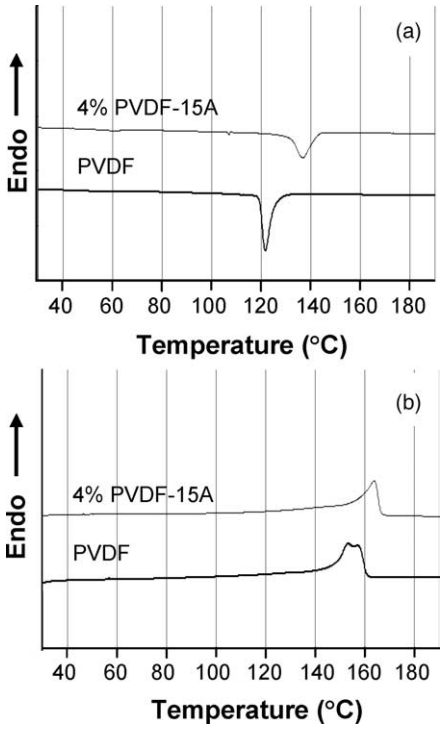

Fig. 11. Crystallization (a) and melting (b) DSC curves for precipitated PVDF and 4% PVDF–15A samples after hot-pressing into films.

experiments (Fig. 12), but instead is the result of the dependence of the melting point of crystallites on lamellar thickness. Interestingly, commercial Kynar® homopolymer PVDF resins show only single melting peak, suggesting that the double peaks could be the result of different head–head and tail–tail isomerism between different PVDF samples. DSC thermograms of PVDF–nanoclay nanocomposites also show single melting peak. This is most likely a result of the nanoclay acting as a heterogeneous nucleating agent for PVDF crystallization and promoting smaller, more uniform lamellae that all melt at the same time during a heating cycle (Section 3.3.3).

3.3.2. In situ thermal wide angle X-ray diffraction

To further confirm that the increased T_c or T_m are a result of the β-phase of the PVDF–nanoclay nanocomposites, in situ thermal WAXD experiments were performed on the entire series of PVDF-layered silicate composites at Brookhaven National Laboratory and results on pure PVDF and PVDF/25A (2%) nanocomposite are shown in Fig. 12. At high temperatures—where all crystalline domains have melted—the WAXD scan shows only an amorphous halo correlating to the average distance between adjacent polymer chains. As the samples cool, crystalline diffraction peaks appear and different diffraction patterns are observed for pure PVDF and PVDF–nanoclay nanocomposites.

Fig. 12 clearly shows that for the PVDF-only sample the three prominent α-phase diffraction peaks first appear at 125 °C

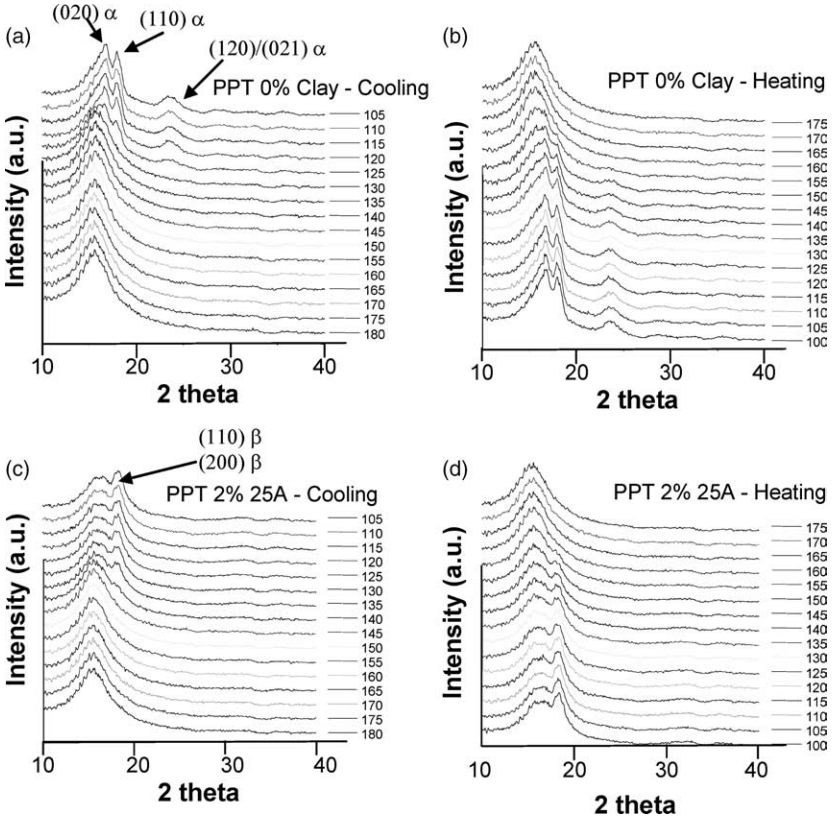

Fig. 12. In situ thermal WAXD data of precipitated PVDF and PVDF–nanoclay nanocomposite samples showing: (a) cooling pristine PVDF sample, (b) cooling a sample containing 2% 25A, (c) heating pristine PVDF sample, (d) heating a sample containing 2% 25A.

as the sample is cooled, while Fig. 12(b) shows the same peaks beginning to melt at 150 °C as the sample is heated. On the other hand, Fig. 12(c) shows the PVDF–nanoclay nanocomposite shows the single prominent β-phase peak first appearing at 140 °C, while Fig. 12(d) shows this peak beginning to melt at 165 °C. This is in complete agreement with the DSC data in Table 1 as both the DSC and the variable temperature WAXD experiments were run at 10 °C/min, which confirms that the increased T_c or T_m of the PVDF–nanoclay nanocomposites is a result of the nanoclay preferentially promoting the growth of the β polymorph over the more common α-phase.

3.3.3. Polarized light microscopy

PLM images provide evidence that supports the effectiveness of the nanoclay as a nucleating agent. In Fig. 13(a), pure PVDF sample crystallized for 6 h at 152 °C shows a bimodal morphology [8,37,38]. Large, strongly birefringent α-phase spherulites are evident from the figure. They are uniform in size, averaging about 60 μm in diameter. Smaller, less birefringent γ-phase spherulites, about 10 μm in diameter, can also be seen in Fig. 13(a). These γ-phase spherulites are very common for PVDF crystallized isothermally at high temperatures for long times [8,37–39]. Their identity as γ-phase was confirmed by slowly heating the sample on the microscopy hot-stage and witnessing that the α-phase spherulites melted about 6 °C lower than the smaller γ-phase spherulites.

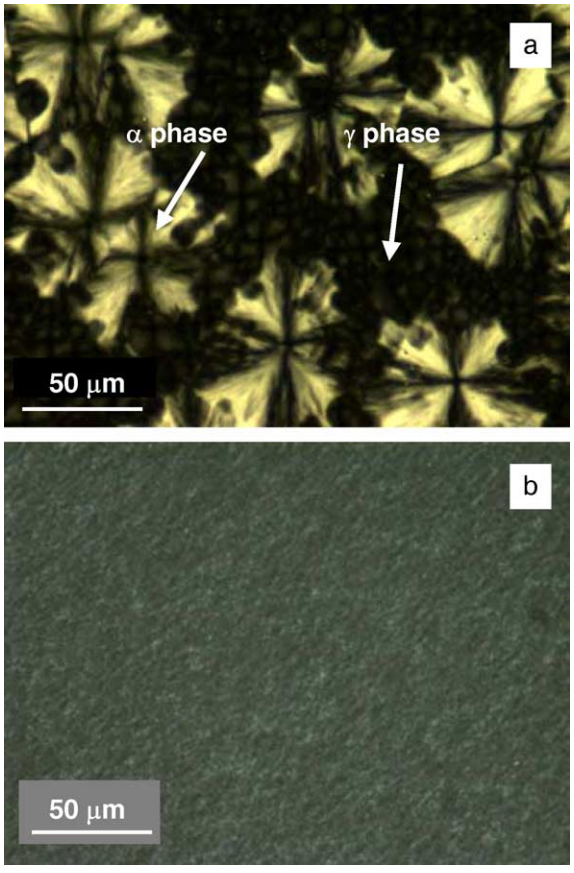

Fig. 13. PLM images of PVDF and PVDF-layered silicate nanocomposites: (a) pristine PVDF spherulites after 6 h at 152 °C, (b) PVDF–15A nanocomposite after 5 h at 162 °C.

However, the PVDF–nanoclay nanocomposite containing 2% 15A shows strikingly different behavior. Fig. 13(b) shows a precipitated PVDF–nanoclay nanocomposite after isothermal crystallization for 5 h at 162 °C. The PVDF–nanoclay nanocomposite exhibits such a small spherulite size that the sample appears nearly uniform grey in color with no measurable dimensions of the spherulites. Other T_cs were also used—both higher and lower—but all showed similar morphologies after crystallization. This suggests that nanoclays act as nucleation sites and physical barriers for PVDF spherulite growth and only small size lamellae could be obtained between the nanoclay layers. This might account for the observation of single melting peaks in nanocomposites while double melt peaks were observed in pure PVDF in DSC heating thermograms.

4. Conclusions

In conclusion, PVDF–nanoclay nanocomposites were successfully prepared by using solution casting and co-precipitation methods. In solution-cast samples, PVDF–15A nanocomposites showed a phase separated morphology while the PVDF–25A nanocomposites are partially intercalated. The nanoclay layers in solution-cast films are aligned parallel to the film surface. This is independent of the morphology of the nanoclay or the organic modifier used. All the co-precipitated nanocomposites were completely exfoliated, indicating that the DMF solution is sufficient to exfoliate the nanoclay, but only fast precipitation of PVDF freezes the metastable exfoliated morphology. The slower kinetics of evaporating solvent from solution cast films permits an intercalated or phase separated structure. PVDF crystallizes in the β polymorph in the presence of nanoclay. This is independent of the nanoclay loading, morphology, or the method of preparation. The PVDF–nanoclay nanocomposites exhibit much smaller crystallites than the large α-phase spherulites that are dominant in pristine PVDF and the addition of any amount of nanoclay from 1 to 6 wt% decreases the PVDF crystallinity from 38% to approximately 34%. This decrease is independent of the type of organic modifier, the nanoclay loading, or the nanoclay morphology.

Acknowledgements

This work was supported by the National Science Foundation (NSF CAREER award, DMR-0239415), 3M and DuPont. Synchrotron experiments were conducted at beamline X27C, NSLS in Brookhaven National Laboratory supported by DOE.

References

[1] Usuki A, Kojima Y, Kawasumi M, Okada A, Fukushima Y, Kurauchi T, et al. J Mater Res 1993;8:1179.

[2] Kojima Y, Usuki A, Kawasumi M, Okada A, Fukushima Y, Kurauchi T, et al. J Mater Res 1993;8:1185.
[3] Dubois P, Alexandre M. Mater Sci Eng 2000;28:1.
[4] Ray SS, Okamoto M. Prog Polym Sci 2003;28:1539.
[5] Giannelis EP, Krishnamoorti JR, Manias E. Adv Polym Sci 1999;118: 108.
[6] Lovinger AJ. Science 1983;220:1115.
[7] Humphrey JS, Amin-Sanayei R, editors. Vinylidene fluoride polymers. New York: Wiley; 2002.
[8] Lovinger AJ. In: Basset DC, editor. Developments in crystalline polymers. Englewood, NJ: Applied Science Publishers Ltd; 1982.
[9] Briber RM, Khoury F. J Polym Sci, Polym Phys 1993;31:1253.
[10] Miller RL. J Polym Sci, Part B: Polym Phys 1976;14:2325.
[11] Grubb DT, Choi KW. J Appl Phys 1981;52:5908.
[12] Okuda K, Yoshida T, Sugita M, Asahina M. J Polym Sci 1967;B5:465.
[13] Toida Y, Chujo R. Polym J 1974;6:191.
[14] Cortili G, Zerbi G. Spectrochim Acta 1967;23A:2216.
[15] Lovinger AJ. Polymer 1981;22:412–3.
[16] Doll WW, Lando JB. J Macromol Sci, Phys 1968;B2:219.
[17] Doll WW, Lando JB. J Macromol Sci, Phys 1970;B4:889.
[18] Matsushige K, Takemura T. J Polym Sci, Polym Phys Ed 1978;16:921.
[19] Matsushige K, Takeichi T. J Cryst Growth 1980;48:343.
[20] Lando JB, Olf HG, Peterlin A. J Polym Sci, A-1 1966;4:941.
[21] Lando JB, Doll WW. J Macromol Sci, Phys 1968;B2:205.
[22] Luongo JP. J Polym Sci, A-2 1972;1119.
[23] Southgate PD. Appl Phys Lett 1976;28:250.
[24] Das-Gupta DK, Doughty K. Appl Phys Lett 1977;31:585.
[25] Das-Gupta DK, Doughty K. J Appl Phys 1978;49:4601.
[26] Kosmynin BP, Gal'perin YL. Vysokomol Soed 1972;A141603.
[27] Gal'perin YL, Kosmynin BP. Vysokomol Soed 1973;A15:2556.
[28] Wang JJ, Li HH, Liu JC, Duan YX, Jiang SD, Yan SK. J Am Chem Soc 2003;125:1496.
[29] Priya L, Jog JP. J Polym Sci, Polym Phys 2002;40:1682.
[30] Priya L, Jog JP. J Polym Sci, Polym Phys 2003;41:31.
[31] Priya L, Jog JP. J Appl Polym Sci 2003;89:2036.
[32] Liu HJ. J Polym Sci, Polym Chem 2002;40:3873.
[33] Kim Y, White JL. 62nd Ann Tech Conf-Soc Plas Eng 2004;3:3798–802.
[34] White JL, Kim Y. J Appl Polym Sci 2004;92:1061–71.
[35] Giannelis EP, Shah D, Maiti P, Gunn E, Schmidt DF, Jiang DD, et al. Adv Mater 2004;16:1173.
[36] Pramoda KP, Mohamed A, Phang IY, Liu T. Polym Int 2005;54:226.
[37] Lovinger AJ. Polymer 1980;21:1317.
[38] Lovinger AJ. J Polym Sci, Polym Phys Ed 1980;18:793.
[39] Lotz B, Cheng SZD. Polymer 2005;46:577.